THE JOURNAL OF PHYSICAL CHEMISTRY C

Article

pubs.acs.org/JPCC

Interfacial Electronic Structure of Methylammonium Lead Iodide Grown on a Mesoporous TiO_2 Layer on F-Doped Tin Oxide Substrate

Yu Kwon Kim,*[,†,‡] Byungwook Jeon,[†] and Hui Joon Park*[,†,§]

[†]Division of Energy Systems Research, [‡]Department of Chemistry, and [§]Department of Electrical and Computer Engineering, Ajou University, Suwon 16499, South Korea

ABSTRACT: Interfacial electronic structure at the perovskite $CH_3NH_3PbI_3/TiO_2$ or $MAPbI_3/TiO_2$ interface has been investigated using a high-resolution synchrotron photoemission spectroscopy. The core levels and valence band spectra of our solution-processed $MAPbI_3$ layers spin-coated on a mesoporous TiO_2 substrate are consistent with a pure iodide perovskite ($MAPbI_3$) with residual methylammonium ($CH_3NH_3^+$) trapped within the perovskite crystal lattice, which is in contact with TiO_2. In addition, we show spectroscopic evidence for the presence of PbI_2 and methylamine (CH_3NH_2) at the $MAPbI_3/TiO_2$ interface. Interestingly, the Fermi level (E_F) aligned to the conduction band minimum (CBM) of both layers is found to be lifted via a band bending which may be attributed to characteristic chemical bonding structures at the interface. The band bending may act as an electron transfer barrier between $MAPbI_3$ and TiO_2. Thus, our findings in interfacial electronic structure of $MAPbI_3$ layers on TiO_2 will be crucial in understanding its photovoltaic performance.

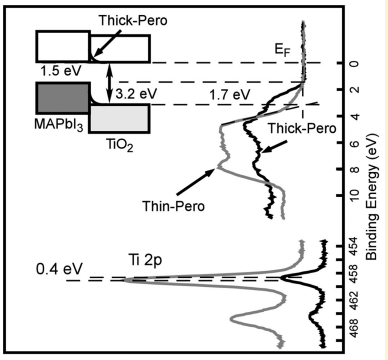

1. INTRODUCTION

Organic−inorganic halide materials such as methylammonium lead halides ($CH_3NH_3PbX_3$, X = I, Cl, Br) have attracted a great deal of attention from many people due to their successful applications as highly efficient photovoltaic materials.[1−3] The attraction is not only due to the cheapness and abundance of the raw materials but also due to many beneficial physical properties such as strong visible-light absorption, long exciton lifetime, high hole conductivity, and easy fabrication process.[4−7] In addition, the bulk structure of those materials are built on the perovskite lattice based on the octahedral cages made of inorganic divalent metals (e.g., Pb^{2+}, Sn^{2+}, and Ge^{2+}) and halide anions (e.g., Cl, Br, and I) and charge-balancing organic units such as a methylammonium cation ($CH_3NH_3^+$, MA^+).[4,8] Thus, changing stoichiometries of cations and anions provide a chance of obtaining perovskite materials with tunable bandgap (E_g) in the whole visible range[6,9] for the design of an efficient photovoltaic cell with high open-circuit voltage (V_{oc}).

Ever since the successful application in solar cells in 2009,[1,10] the optimized synthetic techniques and stack structures have reached a level of efficiency higher than 20%.[11] In general, for an efficient solar cell performance, a stack structure requires the conducting perovskite structure deposited onto a blocking layer such as TiO_2.[11−13] Studies on the interfacial photophysical mechanisms at the heterojunction are in progress and suggest that one of the important reasons of the high efficiency of $MAPbX_3$ perovskite-based solar cells is its long carrier diffusion lengths that can exceed even several micrometers in a $MAPbX_3$ absorber.[14,15] An efficient ultrafast photoexcited electron transfer from $MAPbX_3$ to TiO_2 is also considered to be important to improve the efficiency. Recent studies indicate that characteristics on electron transfer between perovskite and TiO_2 are strongly influenced by the interface electronic structure between the two layers.[16] A diverse range of the charge transfer times (spanning <1 ps to hundreds of ps) and varying efficiencies observed at the heterojunction[5,17,18] may be in part due to the delicate variation in the chemical bonding and electronic structures at the interface. For example, the mixed halide perovskite/TiO_2 interface may be chemically enriched with Cl which may change the bulk phase of the perovskite layer, influencing the overall photoexcitation efficiency.[19,20] Thus, understanding the chemical and electronic properties of the $MAPbX_3/TiO_2$ interface is crucial for improving device optimization. In accordance with the research needs, recent studies are focused on elucidating the electronic structure of the $TiO_2/MAPbI_3$ interface through combined XPS/UPS measurements.[12,13,16,21] XPS has been deliberately employed to explore the interface and bonding structure of the perovskite materials such as vacuum-deposited $MAPb(I_{1-y}Br_y)_3$ and $MAPb(I_{1-y}Cl_y)_3$ films[22] and solution spin-coated $MAPbI_3$ films.[23]

In this study, we investigated the chemical states of the $MAPbI_3/TiO_2$ interface by preparing fairly thin $MAPbI_3$ layers on TiO_2 to be probed by synchrotron photoemission spectroscopy. All the preparation procedures are the same as those for the solution-based real solar cell device fabrication process except that the thickness is controlled to be either thin (a few nm) or thick (~80 nm). Comparing the core levels and the valence band spectra of the two samples revealed that the charge transfer at the interface shifts the band alignment at the interface in a way to inhibit the efficient electron transfer between the two layers.

Received: July 26, 2016
Revised: August 29, 2016
Published: September 21, 2016

DOI: 10.1021/acs.jpcc.6b07476
J. Phys. Chem. C 2016, 120, 22460−22465

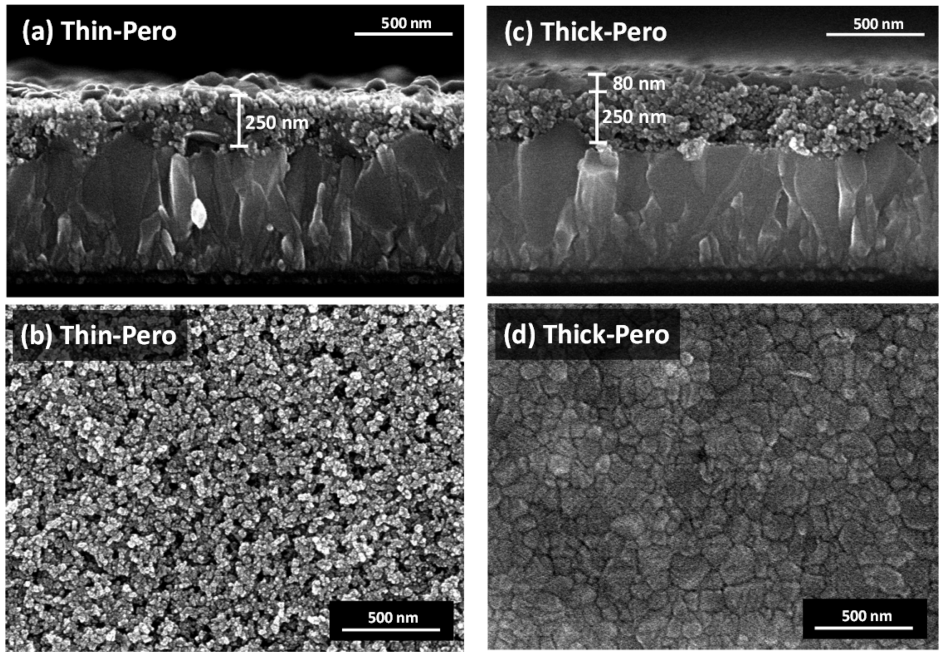

Figure 1. SEM images of the (a, b) thin (Thin-Pero) and (c, d) thick (Thick-Pero) perovskite layers spin-coated on TiO_2/FTO. (a, c) Cross-section view. (b, d) Top view.

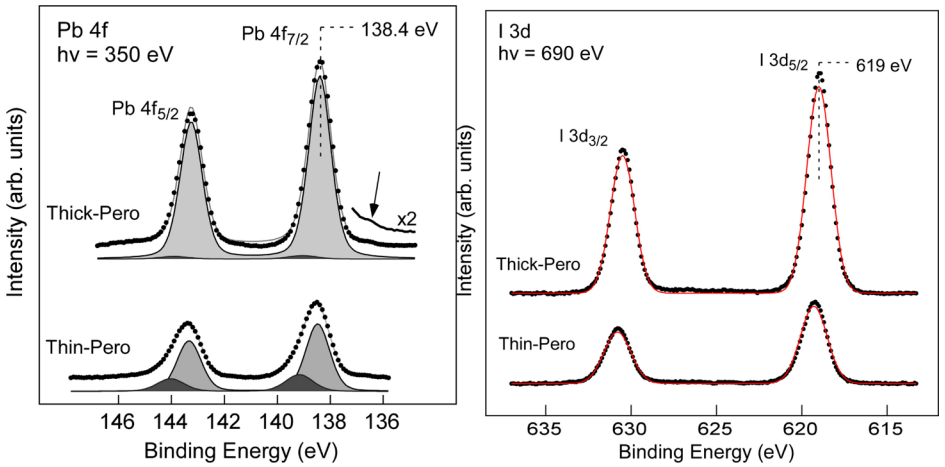

Figure 2. Pb 4f and I 3d core level spectra taken with a photon energy of 350 (690) eV for the thick perovskite film (Thick-Pero, top) and the thin perovskite film (Thin-Pero, bottom).

2. EXPERIMENTAL DETAILS

2.1. Preparation of the $MAPbI_3/TiO_2$/FTO. The fluorine-doped tin oxide (FTO)-coated glass substrates were cleaned by acetone, isopropyl alcohol (IPA), and deionized (DI) water sequentially using ultrasonication. The FTO substrates were treated with O_2 plasma for 3 min prior to use. To prepare the blocking layer TiO_2 on FTO, 0.15 M titanium diisopropoxide bis(acetylacetonate) (75% in 2-propanol, Sigma-Aldrich) was spin-cast on FTO, which was subsequently heated in the furnace at 500 °C for 30 min. This TiO_2 layer prevents the direct contact between FTO and the perovskite photoactive layer. The mesoporous-TiO_2 layer was formed by spin-casting TiO_2 paste (Dyesol), diluted by ethanol (3.5:1 w/w) on blocking-TiO_2/FTO substrate at 5000 rpm for 40 s, followed by an annealing process at 500 °C for 30 min. The $CH_3NH_3PbI_3$ (or $MAPbI_3$) perovskite layer was prepared on the mesoporous-TiO_2 layer as follows. First, CH_3NH_3I was prepared from CH_3NH_2 (24 mL, 33% in ethanol, Sigma-Aldrich) and HI (10 mL, 57 wt % in water, Sigma-Aldrich), which were mixed at 0 °C and stirred for 2 h, and the resulting solution was evaporated by a rotary evaporator at 60 °C for 30 min. The product was dissolved in ethanol and washed by diethyl ether three times. Finally, the product was dried at 70 °C in a vacuum oven for 24 h. The PbI_2 was purchased from Sigma-Aldrich and used as received. PbI_2 and CH_3NH_3I (1:1 molar ratio) were added to the mixture of γ-butyrolactone (GBL) and dimethyl sulfoxide (DMSO) (7:3 v/v) in an inert atmosphere. The solution was stirred at 70 °C for at least 12 h before use. The solution (0.9 M solution for Thick-Pero and 0.6 M solution for Thin-pero) was spin-cast onto the mesoporous-TiO_2/blocking-TiO_2/FTO substrate at 1000 rpm for 10 s and 5000 rpm for 20 s sequentially. During the second spin-casting step, 1 mL of toluene was added onto the substrate. To explore the interface between the perovskite and the TiO_2, the thickness of the perovskite layer was controlled to

DOI: 10.1021/acs.jpcc.6b07476
J. Phys. Chem. C 2016, 120, 22460−22465

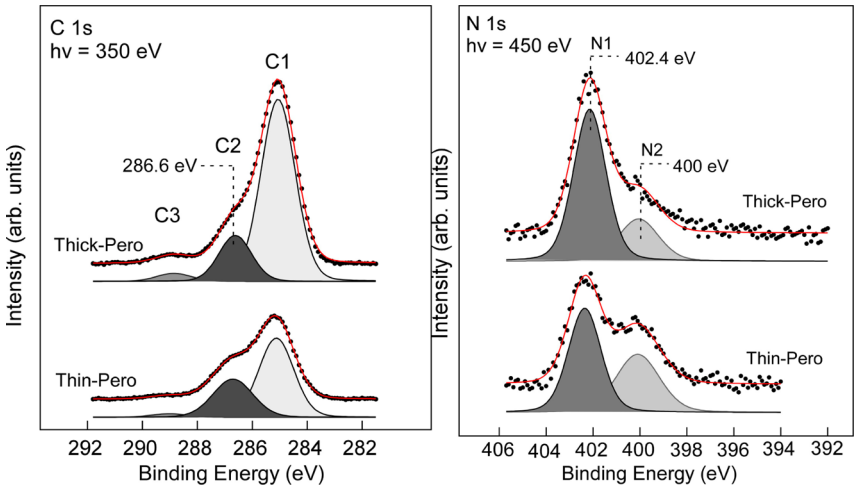

Figure 3. C 1s and N 1s core level spectra taken with a photon energy of 350 (450) eV at normal emission for the thick perovskite film (Thick-Pero, top) and the thin perovskite film (Thin-Pero, bottom).

be either thin (~a few nm, Thin-Pero) or thick (~80 nm, Thick-Pero). After spin-casting, the substrate was annealed at 100 °C for 10 min on a hot plate.

The cross-sectional SEM images as well as the top-view images of the two samples are displayed in Figure 1. The cross-sectional view of Thick-Pero (Figure 1(c)) confirms the thickness of $MAPbI_3$ is about 80 nm. The film, however, is not uniform and has crevices (see Figure 1(c) and (d)) allowing the underlying TiO_2 layer to be seen by XPS. For the case of Thin-Pero, the large area of the TiO_2 layer is directly exposed to the surface with some $MAPbI_3$ particles distributed on the surface. This condition allows us to measure the chemical states of both $MAPbI_3$ and TiO_2 layers and the interfacial states for both samples.

2.2. Photoemission Characterization. All experiments were performed in an UHV chamber attached to the 10D beamline of Pohang Accelerator Laboratory (PAL). The perovskite samples cut into ~5 × 5 mm size were mounted onto a Mo sample holder by wrapping Ta strips around the samples and spot-welding the Ta strips onto the Mo sample holder. A thick Au film of ~5 × 5 mm in size was also attached to the sample holder to be used as a reference for binding energy calibration.

Photoemission spectra of Pb 4f, I 3d, N 1s, C 1s, Ti 2p, and O 1s core levels and valence band were taken using a commercial electron analyzer (PHOIBOS 150, SPECS) at a fixed normal emission geometry at RT. Photon energies were varied at 250−690 eV. The binding energies of the photoemission spectra were determined by taking the binding energy of the Au $4f_{7/2}$ core level to be 84 eV.

3. RESULTS AND DISCUSSION

Figure 2 shows Pb 4f and I 3d core levels taken from the thick (Thick-Pero) and thin (Thin-Pero) perovskite films. The Pb 4f core level shows well-resolved Pb 4f features with spin−orbit split of 4.9 eV. We find that the main Pb 4f feature is centered at 138.4 eV for both cases. However, the detailed spectral shape of Thin-Pero is extended toward higher binding energy, suggesting the presence of another component. Also, we note a small shoulder at 136.7 eV (see the arrow in Figure 2); it is assigned to metallic Pb[24] which is commonly observed from decomposition of $MAPbI_3$.[23] The Pb 4f is fitted with two components at Pb $4f_{7/2}$ binding energies at 138.4 and 139.1 eV, respectively. The peak at 138.4 eV dominates the Pb 4f features of Thick-Pero, while the one at 139.1 eV is enhanced for Thin-Pero. Thus, the high-binding-energy peak must be related to those Pb species at the interface between $MAPbI_3$ and TiO_2. Since the binding energies of Pb^{2+} from $MAPbX_3$ (X = I, Br, Cl) are commonly observed at 138.4−138.7 eV,[22,23,25−27] it is reasonable to assign the one at 138.4 eV to the bulk Pb^{2+} component of the $MAPbI_3$ film. The blue-shifted Pb component (139.1 eV) may be related to oxidized Pb^{3+} species[26] or to PbI_2/TiO_2; a blue shift in the Pb 4f binding energy (to 138.8 eV) is suggested for TiO_2/PbI_2 compared to that of $TiO_2/CH_3NH_3PbI_3$.[13] A tiny amount of residual PbI_2 impurity is often found in the perovskite crystal phase in the $MAPbI_3$-based photoactive layer for high performance solar cells.[21,28−30] The roles of PbI_2 are under intense investigation and are suggested to be either positive (passivation of grain boundary of perovskite crystal,[28] enhancement of the electronic coupling at the interface with TiO_2,[21] or reduction of the trap density at that interface[29]) or negative (electron blocking due to its higher conduction band than perovskite,[30] inducing an intrinsic instability to the film under illumination,[31] or increasing hysteresis[32]). The conflicting roles of PbI_2 may be attributed to different preparation methods which can influence the actual amount and the morphology of the residual PbI_2 in perovskite films. Considering the nonoxidizing condition of our preparation method, it seems also reasonable to assign the 139.1 eV Pb component to PbI_2 predominantly accumulated around the interface with TiO_2.

Also shown in Figure 2 is the I 3d core level which can be fitted with a single component with a characteristic spin−orbit split of 11.5 eV. The I $3d_{5/2}$ binding energy is determined to be 619.1−619.2 eV for both films. The measured I $3d_{5/2}$ binding energies also fall in the range of I^- species observed for $MAPbI_3/TiO_2$ of other groups.[13]

The presence of methylammonium (MA, $CH_3NH_3^+$) in the lattice is evidenced from C 1s and N 1s core levels shown in Figure 3. The C 1s core level features a peak centered at 285 eV with shoulders toward higher binding energies, which are fitted with three components at 285 (C1), 286.6 (C2), and 288.8 (C3) eV, respectively. Although the peak at 285 eV (C1) is a dominant one, it is likely to be C-based contaminants residing at the perovskite/TiO_2 surface since it is commonly observed from the spectra of ex-situ spin-coated samples. The C 1s peak

DOI: 10.1021/acs.jpcc.6b07476
J. Phys. Chem. C 2016, 120, 22460−22465

that is assigned to C species of methylammonium in the perovskite is the one at 286.6 eV after the comparison of the binding energies obtained from other studies.[25,33,34] The small peak at 288.8 eV is likely to be airborne C contaminants such as carbonate species.

N 1s core level spectra in Figure 3 exhibit a major peak at 402.4 eV with a shoulder at lower binding energies. Fitting reveals two components at 402.4 (N1) and 400 (N2) eV, respectively. Very similar N 1s spectral shape with a peak at 402 eV and shoulders toward lower binding energies was also detected for the $CH_3NH_3PbI_{3-x}Cl_x$ perovskite films/Al_2O_3 (and Si)[25] and for $CH_3NH_3PbI_3$ on TiO_2 at 402.7 eV.[33] Also, the N 1s peak at 402 eV has been reported for the MAI/$PbCl_2$ bilayer film in situ deposited on an ITO glass.[34] Thus, the N1 peak can be assigned to N species in methylammonium ($CH_3NH_3^+$) trapped within the perovskite crystal lattice. The N 1s peak close to 400 eV was also observed from molecular methylamine (CH_3NH_2) condensed on metal surfaces as a multilayer[35] or a free terminal NH_2 group as in self-assembled monolayers of S-bound aminethiols on Au.[36] A similar N-containing molecule such as 4-mercaptopyridine bound to TiO_2 may show a N 1s peak at 400−401.5 eV depending on the binding sites (Ti or OH sites).[37] Protonation of the amine group to $-NH_3^+$ species may induce a blue-shift in the N 1s binding energy by about 1−2 eV to 401−402 eV,[38] as has been observed for the MA-based perovskite films.[25,33,34] Interestingly, the ratio of N2 to N1 is higher for Thin-Pero than for Thick-Pero suggesting that N2 is related to those accumulated at the interface or in contact with TiO_2. Thus, the N2 species may be assigned to excess molecular species (such as CH_3NH_2) at the interface accumulated at the interface or bound to TiO_2 during the formation of the perovskite phase.[20]

Figure 4 compares the valence band spectra for the two (thick and thin) perovskite films on TiO_2 taken with various photon energies. We note that the valence band spectra for Thick-Pero show dominant features at 2−5 eV associated with the electronic states of PbI_3^-, while those for Thin-Pero have more pronounced bands at 4−8 eV due to the dominant contribution of the TiO_2 layer in the valence band. The very similar valence band shape with the perovskite features at 2−5 eV has been also reported for the earlier studies on TiO_2/$CH_3NH_3PbI_3$[13] and $CH_3NH_3PbI_2Cl$ perovskite.[24]

The features at 2−5 eV originate from the contribution of the iodides (I 5p) at 3 eV and the Pb−I−Pb bonds with bonding (at ∼5 eV) and antibonding (at valence band edge) states.[8,13] By extrapolating the decaying intensity toward zero (represented by the horizontal baseline), the valence band maximum (VBM) is determined to be about 1.5 eV below the Fermi level (E_F). VBM position of 1.5 eV is very close to the nominal energy gap (1.5−1.6 eV) predicted for the halide perovskite $CH_3NH_3PbI_3$.[8]

For Thin-Pero, the contribution of O 2p at ∼4 eV is especially pronounced for the valence band spectrum taken with the photon energy of 250 eV (see Figure 4) due to the large contribution of the surface-exposed TiO_2 layers. Thus, the VBM of the TiO_2 layer may be obtained by the extrapolation of the decaying edge of the O 2p band, which gives about 3.2 eV below the E_F. The value is very close to the band gap of TiO_2, indicating that the E_F of the TiO_2 is aligned to the bottom of its conduction band. Thus, for the case of Thin-Pero, the Fermi levels of the perovskite and TiO_2 layers are assumed to be aligned to the bottom of their respective conduction band minimums (CBM).

The O 1s and Ti 2p core level spectra for the thin and thick samples are presented in Figure 5. Main spectral features are consistent with that expected from the stoichiometric TiO_2 layer with Ti^{4+} and O^{2-}. The O 1s peak at 530.3 eV for Thin-Pero is assigned to the lattice O^{2-} species of TiO_2. The

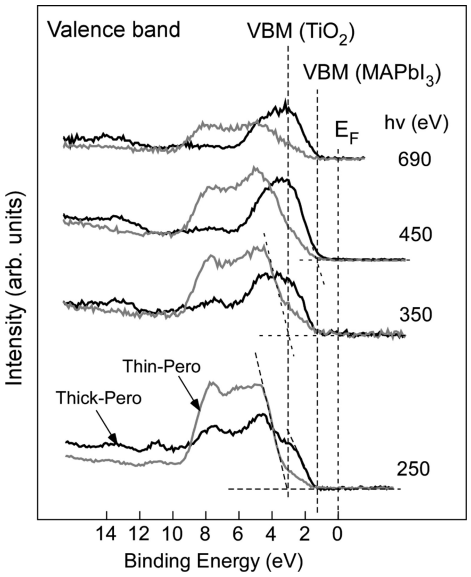

Figure 4. Valence band spectra taken with the photon energies of 250, 350, 450, and 690 eV at normal emission for the thick perovskite film (Thick-Pero, black) and the thin perovskite film (Thin-Pero, gray).

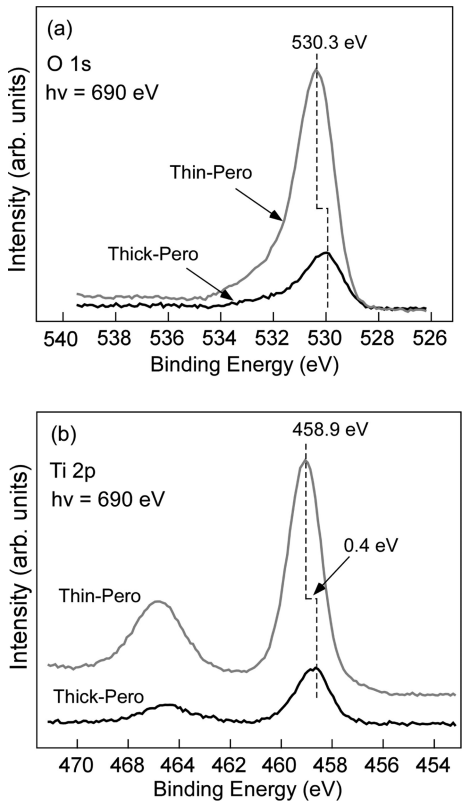

Figure 5. O 1s and Ti 2p core level spectra taken with a photon energy of 690 eV at normal emission for the thin (Thin-Pero, gray) and thick (Thick-Pero, black) perovskite/TiO_2.

DOI: 10.1021/acs.jpcc.6b07476
J. Phys. Chem. C 2016, 120, 22460−22465

asymmetric tail toward high-binding energy extended from 502 to 505 eV is due to oxygen atoms in hydroxyls (−OH) and chemisorbed water, which are blue-shifted by about 1.6 and 2.9 eV, respectively, from the main oxide peak.[39] The oxygen functional groups in airborne contaminants may also contribute to the spectrum and overlap with that from OH. The Ti $2p_{3/2}$ peak at 458.9 eV is assigned to the lattice Ti^{4+} of TiO_2. No distinct low-binding energy tail or shoulder is observed, indicating a stoichiometric TiO_2.

Interestingly, we note the binding energies of Ti 2p and O 1s for Thick-Pero are shifted toward lower binding energies by about 0.4 eV compared to those for Thin-Pero, while Pb 4f and I 3d core levels are not (see Figure 2). The unambiguous shift in the binding energies of the Ti 2p and O 1s core levels from the skin-depth layers of TiO_2 underneath the perovskite layer between Thin-Pero and Thick-Pero can be understood from the fact that the Fermi level of the sample holder (and the Au foil) is aligned to that of the top perovskite layer. Thin-Pero has a perovskite-free TiO_2 layer mostly exposed to the surface; most of the surface of Thick-Pero is covered with the perovskite layer, and the exposed TiO_2 layer should be in contact with the perovskite layer. Thus, the observed core level shifts of the TiO_2 layer from Thick-Pero compared to those of Thin-Pero explain the upward shift of the core levels of TiO_2 for Thick-Pero; the core level shifts of the underlying TiO_2 layer are a result of a shift in the band alignment at the interface between the perovskite and TiO_2 layers. The observed decrease in the binding energies of the Ti 2p and O 1s core levels for Thick-Pero indicates an upward shift of TiO_2 at the interface. The origin for the observed shift can come from a number of influences such as a possible charge transfer to the TiO_2 layer or the introduction of gap states at the interface of perovskite and TiO_2 due to surface defects; any change in the charge state at the surface or interface of TiO_2 can induce a shift of Fermi level and the related core level binding energies.[40−42] Although the origin of the band bending may require additional intense research efforts and is beyond the scope of the present study, here we certainly note the importance of the possible change in the final band alignment between the two layers depending on the detailed chemical bonding structure at the interface of the perovskite and TiO_2 layers. The shift in the band alignment at the $MAPbI_3/TiO_2$ interface may have a strong influence on the photovoltaic performance at the interface. For example, an earlier report suggests that the interfacial dipole formed at the $MAPbI_3/TiO_2$ interface may act as an electron-transfer barrier and limit the overall photovoltaic efficiency.[16]

4. CONCLUSIONS

In conclusion, after a systematic comparison of core levels and valence band spectra for the thick and thin $MAPbI_3/TiO_2$, we find important characteristics in the electronic structure at the interface. The new interfacial bonding state of Pb is observed and is assigned to residual PbI_2 predominantly accumulated at the interface with TiO_2. The N 1s core level also reveals an interfacial nitrogen species associated with methylamine bound at the interface. Valence band spectra show that the VBM is about 1.5 eV below E_F for both cases, suggesting that the CBM of the perovskite layer is aligned to the Au reference foil. The valence band features of TiO_2 are resolved for Thin-Pero, allowing a construction of relative band alignment between the two layers; the E_F's are aligned to the CBMs of the perovskite and TiO_2 layers. For the Thick-Pero, however, we find that the charge transfer from the perovskite layer to TiO_2 induces an upward band bending of the VB and CB of TiO_2 at the interface and shifts the E_F of TiO_2 lower in the band gap; this results in an electron transfer barrier and may limit the overall photovoltaic performance.

AUTHOR INFORMATION

Corresponding Authors

*Phone: 82-31-219-2896. Fax: 82-31-219-2969. E-mail: yukwonkim@ajou.ac.kr.

*Phone: 82-31-219-2577. Fax: 82-31-219-2208. E-mail: huijoon@ajou.ac.kr.

Notes

The authors declare no competing financial interest.

ACKNOWLEDGMENTS

This research was supported by the Basic Science Research Program through the National Research Foundation of Korea (NRF), funded by the Ministry of Education (NRF-2014R1A1A2056403). This work is also supported by "Human Resources Program in Energy Technology" of the Korea Institute of Energy Technology Evaluation and Planning (KETEP), granted financial resource from the MOTIE, Republic of Korea (Project No: 2015 4010 200820).

REFERENCES

(1) Kim, H.-S.; Lee, C.-R.; Im, J.-H.; Lee, K.-B.; Moehl, T.; Marchioro, A.; Moon, S.-J.; Humphry-Baker, R.; Yum, J.-H.; Moser, J. E.; et al. Lead Iodide Perovskite Sensitized All-Solid-State Submicron Thin Film Mesoscopic Solar Cell with Efficiency Exceeding 9%. *Sci. Rep.* **2012**, *2*, 591.

(2) Lee, M. M.; Teuscher, J.; Miyasaka, T.; Murakami, T. N.; Snaith, H. J. Efficient Hybrid Solar Cells Based on Meso-Superstructured Organometal Halide Perovskites. *Science* **2012**, *338*, 643−647.

(3) Jeon, S.; Thakur, U. K.; Lee, D.; Wenping, Y.; Kim, D.; Lee, S.; Ahn, T. K.; Park, H. J.; Kim, B.-G. N-phenylindole-Diketopyrrolo-pyrrole-Containing Narrow Band-Gap Materials for Dopant-Free Hole Transporting Layer of Perovskite Solar Cell. *Org. Electron.* **2016**, *37*, 134−140.

(4) Green, M. A.; Ho-Baillie, A.; Snaith, H. J. The Emergence of Perovskite Solar Cells. *Nat. Photonics* **2014**, *8*, 506−514.

(5) Marchioro, A.; Teuscher, J.; Friedrich, D.; Kunst, M.; van de Krol, R.; Moehl, T.; Grätzel, M.; Moser, J.-E. Unravelling the Mechanism of Photoinduced Charge Transfer Processes in Lead Iodide Perovskite Solar Cells. *Nat. Photonics* **2014**, *8*, 250−255.

(6) Noh, J. H.; Im, S. H.; Heo, J. H.; Mandal, T. N.; Seok, S. I. Chemical Management for Colorful, Efficient, and Stable Inorganic−Organic Hybrid Nanostructured Solar Cells. *Nano Lett.* **2013**, *13*, 1764−1769.

(7) Kwon, U.; Kim, B.-G.; Nguyen, D. C.; Park, J.-H.; Ha, N. Y.; Kim, S.-J.; Ko, S. H.; Lee, S.; Lee, D.; Park, H. J. Solution-Processible Crystalline NiO Nanoparticles for High-Performance Planar Perovskite Photovoltaic Cells. *Sci. Rep.* **2016**, *6*, 30759.

(8) Bretschneider, S. A.; Weickert, J.; Dorman, J. A.; Schmidt-Mende, L. Research Update: Physical and Electrical Characteristics of Lead Halide Perovskites for Solar Cell Applications. *APL Mater.* **2014**, *2*, 040701.

(9) Castelli, I. E.; García-Lastra, J. M.; Thygesen, K. S.; Jacobsen, K. W. Bandgap Calculations and Trends of Organometal Halide Perovskites. *APL Mater.* **2014**, *2*, 081514.

(10) Kojima, A.; Teshima, K.; Shirai, Y.; Miyasaka, T. Organometal Halide Perovskites as Visible-Light Sensitizers for Photovoltaic Cells. *J. Am. Chem. Soc.* **2009**, *131*, 6050−6051.

(11) Saliba, M.; Orlandi, S.; Matsui, T.; Aghazada, S.; Cavazzini, M.; Correa-Baena, J.-P.; Gao, P.; Scopelliti, R.; Mosconi, E.; Dahmen, K.-H.; et al. A Molecularly Engineered Hole-Transporting Material for Efficient Perovskite Solar Cells. *Nat. Energy* **2016**, *1*, 15017.

DOI: 10.1021/acs.jpcc.6b07476
J. Phys. Chem. C 2016, 120, 22460−22465

(12) Ke, W.; Fang, G.; Wang, J.; Qin, P.; Tao, H.; Lei, H.; Liu, Q.; Dai, X.; Zhao, X. Perovskite Solar Cell with an Efficient TiO_2 Compact Film. *ACS Appl. Mater. Interfaces* **2014**, *6*, 15959−15965.
(13) Lindblad, R.; Bi, D.; Park, B.-W.; Oscarsson, J.; Gorgoi, M.; Siegbahn, H.; Odelius, M.; Johansson, E. M. J.; Rensmo, H. Electronic Structure of $TiO_2/CH_3NH_3PbI_3$ Perovskite Solar Cell Interfaces. *J. Phys. Chem. Lett.* **2014**, *5*, 648−653.
(14) Stranks, S. D.; Eperon, G. E.; Grancini, G.; Menelaou, C.; Alcocer, M. J. P.; Leijtens, T.; Herz, L. M.; Petrozza, A.; Snaith, H. J. Electron-Hole Diffusion Lengths Exceeding 1 Micrometer in an Organometal Trihalide Perovskite Absorber. *Science* **2013**, *342*, 341−344.
(15) Dong, Q.; Fang, Y.; Shao, Y.; Mulligan, P.; Qiu, J.; Cao, L.; Huang, J. Electron-Hole Diffusion Lengths > 175 μm in Solution-Grown $CH_3NH_3PbI_3$ Single Crystals. *Science* **2015**, *347*, 967−970.
(16) Xing, G.; Wu, B.; Chen, S.; Chua, J.; Yantara, N.; Mhaisalkar, S.; Mathews, N.; Sum, T. C. Interfacial Electron Transfer Barrier at Compact $TiO_2/CH_3NH_3PbI_3$ Heterojunction. *Small* **2015**, *11*, 3606−3613.
(17) Zhu, Z.; Ma, J.; Wang, Z.; Mu, C.; Fan, Z.; Du, L.; Bai, Y.; Fan, L.; Yan, H.; Phillips, D. L.; Yang, S. Efficiency Enhancement of Perovskite Solar Cells through Fast Electron Extraction: The Role of Graphene Quantum Dots. *J. Am. Chem. Soc.* **2014**, *136*, 3760−3763.
(18) Ponseca, C. S.; Savenije, T. J.; Abdellah, M.; Zheng, K.; Yartsev, A.; Pascher, T.; Harlang, T.; Chabera, P.; Pullerits, T.; Stepanov, A.; et al. Organometal Halide Perovskite Solar Cell Materials Rationalized: Ultrafast Charge Generation, High and Microsecond-Long Balanced Mobilities, and Slow Recombination. *J. Am. Chem. Soc.* **2014**, *136*, 5189−5192.
(19) Wang, Q.; Lyu, M.; Zhang, M.; Yun, J.-H.; Chen, H.; Wang, L. Transition from the Tetragonal to Cubic Phase of Organohalide Perovskite: The Role of Chlorine in Crystal Formation of $CH_3NH_3PbI_3$ on TiO_2 Substrates. *J. Phys. Chem. Lett.* **2015**, *6*, 4379−4384.
(20) Yu, H.; Wang, F.; Xie, F.; Li, W.; Chen, J.; Zhao, N. The Role of Chlorine in the Formation Process of "$CH_3NH_3PbI_{3-x}Cl_x$" Perovskite. *Adv. Funct. Mater.* **2014**, *24*, 7102−7108.
(21) Mosconi, E.; Grancini, G.; Roldán-Carmona, C.; Gratia, P.; Zimmermann, I.; Nazeeruddin, M. K.; De Angelis, F. Enhanced TiO_2/$MAPbI_3$ Electronic Coupling by Interface Modification with PbI_2. *Chem. Mater.* **2016**, *28*, 3612−3615.
(22) Kim, T. G.; Seo, S. W.; Kwon, H.; Hahn, J.; Kim, J. W. Influence of Halide Precursor Type and Its Composition on the Electronic Properties of Vacuum Deposited Perovskite Films. *Phys. Chem. Chem. Phys.* **2015**, *17*, 24342−24348.
(23) Liu, P.; Liu, X.; Lyu, L.; Xie, H.; Zhang, H.; Niu, D.; Huang, H.; Cheng, B.; Xiao, Z.; Huang, J.; et al. Interfacial Electronic Structure at the $CH_3NH_3PbI_3/MoO_x$ Interface. *Appl. Phys. Lett.* **2015**, *106*, 193903.
(24) Conings, B.; Baeten, L.; De Dobbelaere, C.; D'Haen, J.; Manca, J.; Boyen, H.-G. Perovskite-Based Hybrid Solar Cells Exceeding 10% Efficiency with High Reproducibility Using a Thin Film Sandwich Approach. *Adv. Mater.* **2014**, *26*, 2041−2046.
(25) Calloni, A.; Abate, A.; Bussetti, G.; Berti, G.; Yivlialin, R.; Ciccacci, F.; Duò, L. Stability of Organic Cations in Solution-Processed $CH_3NH_3PbI_3$ Perovskites: Formation of Modified Surface Layers. *J. Phys. Chem. C* **2015**, *119*, 21329−21335.
(26) Pederson, L. R. Two-Dimensional Chemical-State Plot for Lead Using XPS. *J. Electron Spectrosc. Relat. Phenom.* **1982**, *28*, 203−209.
(27) Barr, T. L.; Yin, M.; Varma, S. Detailed X-Ray Photoelectron Spectroscopy Valence Band and Core Level Studies of Select Metals Oxidations. *J. Vac. Sci. Technol., A* **1992**, *10*, 2383−2390.
(28) Chen, Q.; Zhou, H.; Song, T.-B.; Luo, S.; Hong, Z.; Duan, H.-S.; Dou, L.; Liu, Y.; Yang, Y. Controllable Self-Induced Passivation of Hybrid Lead Iodide Perovskites toward High Performance Solar Cells. *Nano Lett.* **2014**, *14*, 4158−4163.
(29) Bi, D.; Tress, W.; Dar, M. I.; Gao, P.; Luo, J.; Renevier, C.; Schenk, K.; Abate, A.; Giordano, F.; Correa Baena, J.-P.; et al. Efficient Luminescent Solar Cells Based on Tailored Mixed-Cation Perovskites. *Sci. Adv.* **2016**, *2*, e1501170.
(30) Lee, Y. H.; Luo, J.; Humphry-Baker, R.; Gao, P.; Grätzel, M.; Nazeeruddin, M. K. Unraveling the Reasons for Efficiency Loss in Perovskite Solar Cells. *Adv. Funct. Mater.* **2015**, *25*, 3925−3933.
(31) Liu, F.; Dong, Q.; Wong, M. K.; Djurišić, A. B.; Ng, A.; Ren, Z.; Shen, Q.; Surya, C.; Chan, W. K.; Wang, J.; et al. Is Excess PbI_2 Beneficial for Perovskite Solar Cell Performance? *Adv. Energy Mater.* **2016**, *6*, 1502206.
(32) Heo, J. H.; Song, D. H.; Han, H. J.; Kim, S. Y.; Kim, J. H.; Kim, D.; Shin, H. W.; Ahn, T. K.; Wolf, C.; Lee, T.-W.; et al. Planar $CH_3NH_3PbI_3$ Perovskite Solar Cells with Constant 17.2% Average Power Conversion Efficiency Irrespective of the Scan Rate. *Adv. Mater.* **2015**, *27*, 3424−3430.
(33) Chen, S.; Goh, T. W.; Sabba, D.; Chua, J.; Mathews, N.; Huan, C. H. A.; Sum, T. C. Energy Level Alignment at the Methylammonium Lead Iodide/Copper Phthalocyanine Interface. *APL Mater.* **2014**, *2*, 081512.
(34) Ng, T.-W.; Chan, C.-Y.; Lo, M.-F.; Guan, Z. Q.; Lee, C.-S. Formation Chemistry of Perovskites with Mixed Iodide/Chloride Content and the Implications on Charge Transport Properties. *J. Mater. Chem. A* **2015**, *3*, 9081−9085.
(35) Chen, J. J.; Winograd, N. The Adsorption and Decomposition of Methylamine on Pd{111}. *Surf. Sci.* **1995**, *326*, 285−300.
(36) Dietrich, P. M.; Graf, N.; Gross, T.; Lippitz, A.; Krakert, S.; Schüpbach, B.; Terfort, A.; Unger, W. E. S. Amine Species on Self-Assembled Monolayers of ω-Aminothiolates on Gold as Identified by XPS and NEXAFS Spectroscopy. *Surf. Interface Anal.* **2010**, *42*, 1184−1187.
(37) Calloni, A.; Brambilla, A.; Berti, G.; Bussetti, G.; Canesi, E. V.; Binda, M.; Petrozza, A.; Finazzi, M.; Ciccacci, F.; Duò, L. X-Ray Photoemission Spectroscopy Investigation of the Interaction between 4-Mercaptopyridine and the Anatase TiO_2 Surface. *Langmuir* **2013**, *29*, 8302−8310.
(38) Song, X.; Ma, Y.; Wang, C.; Dietrich, P. M.; Unger, W. E. S.; Luo, Y. Effects of Protonation, Hydrogen Bonding, and Photo-damaging on X-Ray Spectroscopy of the Amine Terminal Group in Aminothiolate Monolayers. *J. Phys. Chem. C* **2012**, *116*, 12649−12654.
(39) McCafferty, E.; Wightman, J. P. Determination of the Concentration of Surface Hydroxyl Groups on Metal Oxide Films by a Quantitative XPS Method. *Surf. Interface Anal.* **1998**, *26*, 549−564.
(40) Mao, X.; Lang, X.; Wang, Z.; Hao, Q.; Wen, B.; Ren, Z.; Dai, D.; Zhou, C.; Liu, L.-M.; Yang, X. Band-Gap States of TiO_2(110): Major Contribution from Surface Defects. *J. Phys. Chem. Lett.* **2013**, *4*, 3839−3844.
(41) Yang, Z.; Wu, R.; Goodman, D. W. Structural and Electronic Properties of Au on TiO_2(110). *Phys. Rev. B: Condens. Matter Mater. Phys.* **2000**, *61*, 14066.
(42) Kao, C. C.; Tsai, S. C.; Bahl, M. K.; Chung, Y. W. Electronic Properties, Structure and Temperature-Dependent Composition of Nickel Deposited on Rutile Titanium Dioxide (110) Surfaces. *Surf. Sci.* **1980**, *95*, 1−14.

DOI: 10.1021/acs.jpcc.6b07476
J. Phys. Chem. C 2016, 120, 22460−22465